Corrosion Science 174 (2020) 108811

Contents lists available at ScienceDirect

Corrosion Science

journal homepage: www.elsevier.com/locate/corsci

Electrochemical behaviour of 22MnB5 steel coated with hot-dip Al-Si before and after hot-stamping process investigated by means of scanning Kelvin probe microscopy

Camila Pucci Couto[a,b,c,*], Reynier I. Revilla[b], Marco Antonio Colosio[d], Isolda Costa[a], Zehbour Panossian[c], Iris De Graeve[b], Herman Terryn[b], Jesualdo Luiz Rossi[a]

[a] Nuclear and Energy Research Institute, Materials Science and Technology Centre, Av. Prof. Lineu Prestes 2242, 05508-000, São Paulo, Brazil
[b] Vrije Universiteit Brussel, Department of Chemistry and Materials, Research Group of Electrochemical and Surface Engineering, Pleinlaan 2, 1050, Brussels, Belgium
[c] Institute for Technological Research, Laboratory for Corrosion and Protection, Av. Prof. Almeida Prado 532, 05508-901, São Paulo, Brazil
[d] General Motors Mercosul, Av. do Estado 2880, 09550-900, São Caetano do Sul, Brazil

ARTICLE INFO

Keywords:
hot stamping
Hot-dip Al-Si
Galvanic coupling
Electrochemical behaviour
SKPFM

ABSTRACT

Press-hardened steels are commonly protected with hot-dip Al-Si coating. Due to the electrochemical complexity of this system, either before or after hot-stamping process, SKPFM was used to investigate the influence of the thermo-mechanical process on the electrochemical behaviour of the galvanic coupling. The hot-stamping process changed significantly the anodic/cathodic coupling of the coating/steel due to iron enrichment in the coating layer. Hence, a concurrent mechanism was thoroughly established, i.e., while the press hardening enhances the corrosion properties of the steel system (steel and metallic coating) through diffusion, at the same time it diminishes the cathodic protection of the Al-Si layer.

1. Introduction

Advanced high-strength steels (AHSS) and ultra-high-strength steels (UHSS) are strategic materials for the automakers in body-in-white (BIW) applications. The use of these materials allows that the automotive industry attends the demands for lightweight structures, aiming at reducing fuel consumption and at improving safety and crash-worthiness properties. Due to the reduced thickness and the higher tensile strength of AHSS and UHSS in comparison with conventional steels, they have become the current trend for new vehicles [1–4].

When the strength increases, the plastic forming of metals may decrease and a springback effect appears due to residual stresses. Consequently, in order to improve the deformation of AHSS and UHSS, the hot-forming process has been used [5]. Hot stamping is a thermo-mechanical process where steel blank is heated for a few minutes up to austenitization temperatures and then, transferred from furnace to a press tool (die set). The design of the die consists of a water-cooling system which allows that the steel blank is formed and quenched at the same time [1,6–9]. As an industrial process, the soaking temperature and the time as well as the transfer time and the cooling rate may vary among manufacturers. In previous studies, it had been reported that the process range for heating temperature is from 880 °C to 950 °C, the soaking time varies from 3 min to 13 min, the transfer step may take 7 s maximum and the cooling rate must be at least 27 $K{\cdot}s^{-1}$ [1,3,10–13].

The boron-manganese steel has been pointed out as the most suitable material for the hot-stamping process [1]. The 22MnB5 is a widely used steel grade in automotive industries for hot-stamping applications. Before the hot-forming process, the steel consists of a ferrite-pearlite microstructure and shows a tensile strength about 600 MPa. At the end of the thermo-mechanical process, the steel microstructure may become fully martensitic and the tensile strength reaches approximately 1500 MPa [1,8,9,14,15]. Depending on the steel grade, the tensile strength may reach 2000 MPa [1]. Boron-manganese steel combined with the hot-stamping process is known as press-hardened steel (PHS). The production of PHS components has been increasing since early 2000 and the prediction is that, in the next few years, about 600 millions of PHS parts will be worldwide produced [16,17].

The press-hardened steel is commonly protected with metallic coatings prior to hot-stamping process in order to avoid both, steel oxidation and decarburization during the furnace heating and the transfer step to the die press. The hot-dip aluminium-silicon (Al-Si) coating is a widespread system used in steel for hot-stamping

* Corresponding author at: Nuclear and Energy Research Institute, Materials Science and Technology Centre, Av. Prof. Lineu Prestes 2242, 05508-000, São Paulo, Brazil.
E-mail addresses: camila.puccicouto@usp.br, Camila.Pucci.Couto@vub.be (C.P. Couto).

https://doi.org/10.1016/j.corsci.2020.108811
Received 5 March 2020; Received in revised form 15 May 2020; Accepted 9 June 2020
Available online 11 June 2020
0010-938X/

applications. The chemical composition of the coating comprises aluminium and about 10 % Si (in mass). This coating shows stability at high temperature, good corrosion resistance and adhesion, either with the steel substrate or the paint to be applied [1,12,15,18,19]. Nevertheless, even though several studies have been dedicated to hot-stamping applications [3,6,12,18], there are still some open questions concerning the corrosion behaviour of PHS.

The synergy of the barrier effect and the cathodic protection mechanism of metallic coatings guarantee the integrity of metallic components in an economical and safe way [20]. Metallic coatings, such as Mg, Zn and Al-based systems, might provide cathodic protection to the steel substrate by galvanic coupling corrosion mechanism. In this mechanism, the cathodic protection is achieved by supplying the electrons to the steel substrate (cathode). The driving force to provide cathodic protection is the difference of (corrosion) potential between the anode and cathode. In this scenery, the anode is known as sacrificial anode, which is less noble than the cathode, and corrodes preferentially. The higher the difference of potential, the higher the driving force for cathodic protection [20–24].

The corrosion resistance of coated hot-stamped components has been evaluated mostly by means of accelerated tests [3,6]. Allély et al. [3] used different accelerated tests which resulted in different corrosion products formed depending on the test conditions. The corrosion products formed can act as a protective barrier against corrosion. They also concluded that the coating does not provide cathodic protection due to the small potential difference between the coating and the steel substrate, verified by means of electrochemical measurements. Dosdat et al. [6] also compared the corrosion resistance of bare steel, PHS coated with Al-Si and PHS protected with Zn-based coatings (galvanized and galvannealed), using accelerated tests. They highlighted that the red rust criteria cannot be used to evaluate corrosion damages for PHS due to the high amount of iron at the surface of the material, which diffuses during the thermal cycle of hot stamping from the steel substrate towards the coating. The authors showed that the PHS Zn-based coated presented the highest cosmetic and cut-edge corrosion resistance. However, in terms of perforation, both PHS Al-Si and Zn-based showed a similar behaviour. Despite the results, Al-Si was pointed out as the most suitable system for hot-stamping applications due to its cost/efficiency ratio.

The standard electrochemical measurements show the overall behaviour of the sample conditions in different corrosive media. However, due to the complexity of the metallic coating system, either before or after the hot-stamping process, local electrochemical measurements are required in order to evaluate the effect of each sub layer at the cross section on the corrosion resistance. Hence, this study aims at investigating the effect of the hot-stamping process on the electrochemical behaviour of 22MnB5 steel coated with hot-dip Al-Si (10 % Si in mass nominal) by means of general and localized electrochemical techniques, with a special focus on the influence of each sub layer of the metallic coating on the corrosion behaviour.

2. Experimental

2.1. Samples

The industrial based samples in different conditions were evaluated in this study. The details of samples are shown in Table 1.

Table 1
Identification and condition of the different samples evaluated.

Sample	Condition
22MnB5 steel	22MnB5 bare steel
as received Al-Si	22MnB5 steel coated with hot-dip Al-Si (10 % Si in mass)
PHS	as received Al-Si submitted to the hot-stamping process

The samples were cut-off from either the steel sheet or from a door beam, a structural car component, cleaned in isopropyl alcohol and dried in a cold stream of air. The samples' cross-section thickness was 1.4 mm. The samples were prepared according to standard metallographic procedures, including mounting, grinding and polishing.

2.2. Electrochemical measurements

Electrochemical tests were performed using a three-electrode cell which consists of an Ag|AgCl 3 mol·L^{-1} KCl as a reference electrode (RE), a platinum grid as a counter electrode (CE) and the sample as a working electrode (WE). The open circuit potential (OCP) was measured in NaCl solutions with 5.0 % and 3.5 % (in mass) for 1 h. After OCP measurements, anodic polarization curves were obtained, starting from 20 mV below the OCP using a sweep rate of 1 mV·s^{-1}. All tests were carried out at room temperature and the working electrode surface was a circular region with 1 cm of diameter. As received Al-Si and PHS samples were also immersed in 3.5 % (in mass) NaCl solution for 120 min. The samples were removed from the solution after 10 min, 30 min, 60 min and 120 min of exposure and then rinsed in deionized water and dried in a cold stream of air.

2.3. Coating characterization and scanning Kelvin probe force microscopy

The characterization of as received Al-Si and PHS samples, top surface and cross-section, was carried out using a field emission-scanning electron microscope (FE-SEM). FE-SEM images were obtained in secondary electron and backscattering modes and the mappings of the chemical composition were undertaken by means of energy dispersive X-ray spectroscopy (EDS). The microscope was set to operate with a 15 kV acceleration voltage, a 30 pA probe current and a work distance of 10 mm.

The Volta potential and topography analyses were carried out by means of a scanning Kelvin probe force microscopy (SKPFM) technique at a commercial atomic force microscope. These measurements were performed under ambient conditions using rectangular conductive cantilevers with a Pt/Ir coating, a resonant frequency of 50 kHz–70 kHz and a spring constant of 1 N m^{-1} to 5 N m^{-1}. Moreover, highly oriented pyrolytic graphite (HOPG) was used as a reference material for the calibration of the measured Volta potential. Topographic and corresponding potential images were simultaneously obtained using a dynamic mode with a single pass methodology. The potential signal recorded was mathematically inverted (multiplied by -1) in order to reflect the true relation of the Volta potential values and the surface under investigation [25–28]. This procedure is done because during the Volta potential acquisition a feedback voltage signal is applied to the tip instead of the sample. Therefore, the signal recorded is the potential of the tip minus the potential of the sample's surface. Once the signal inversion is done, the Volta potential maps will be in accordance with the electrochemical nobility of the metals (galvanic series). For instance, high potentials will indicate cathodic areas, whereas low potentials will represent more anodic areas [29]. Furthermore, the distribution of Volta potential will be represented by means of histograms. The histograms were constructed based on the Volta potential map, correspondent to a scanned area of 40 × 40 μm^2 which corresponds to a mapping of 512 pixels × 512 pixels. Each pixel represents a potential value. Therefore, each histogram is constructed with 512 × 512 of potential. The intensity represents the count frequency.

3. Results and discussion

3.1. Coating characterization

3.1.1. Surface characterization

The surface morphologies of both, as received Al-Si and PHS samples, are shown in Fig. 1. According to Fig. 1(a) the morphology of the

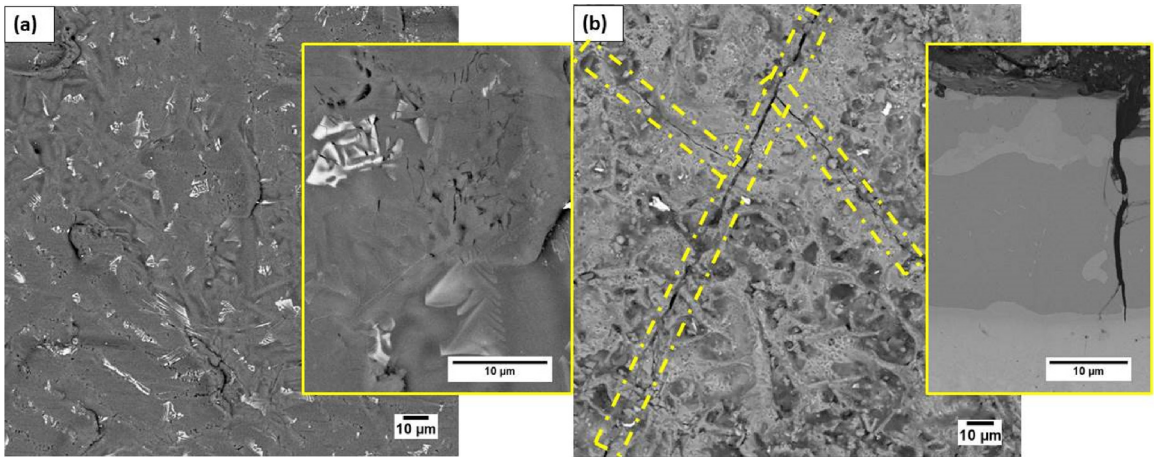

Fig. 1. Scanning backscattered image showing the surface morphology of (a) as received Al-Si with the presence of precipitates (white contrast) and inset image in the right showing the precipitates in higher magnification; (b) PHS sample showing cracks delimited by dashed yellow lines and a zoom-in cross-section image attached in order to highlight the depth that the cracks may reach (For interpretation of the references to colour in this figure legend, the reader is referred to the web version of this article).

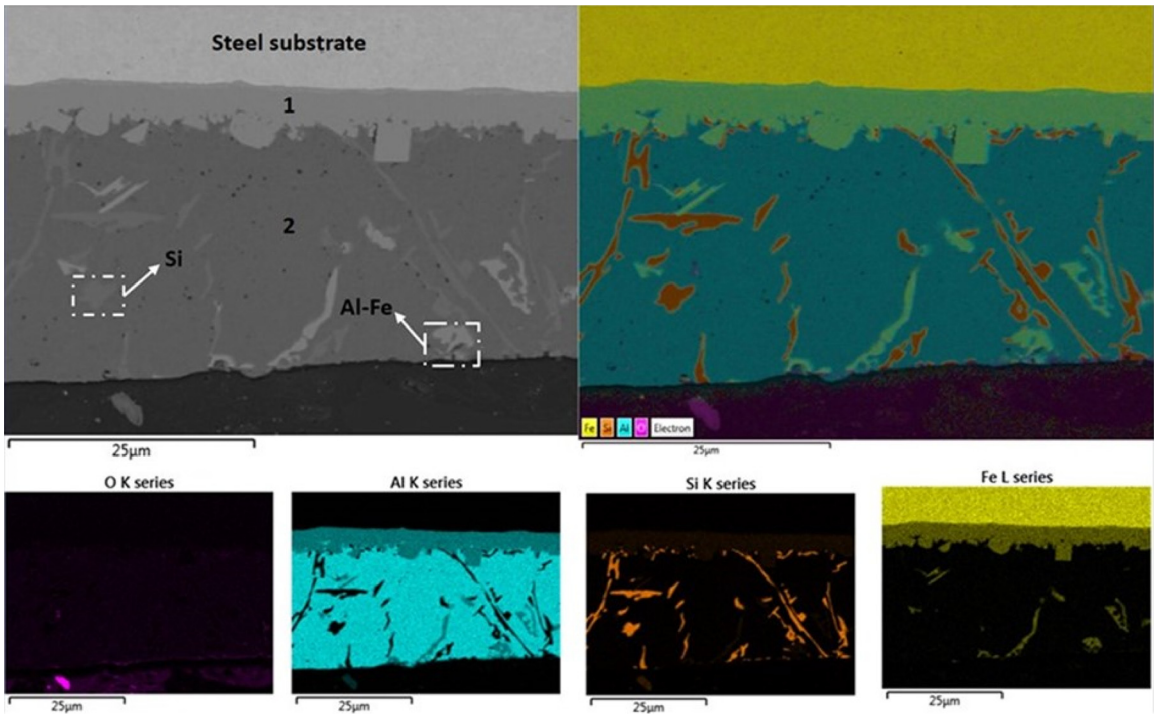

Fig. 2. Scanning backscattered images and EDS elemental mapping of the cross section of the as received Al-Si coated sample for O, Al, Si and Fe.

coating surface of the as received Al-Si sample consists of a homogeneous matrix with some precipitates, which are randomly distributed. There is an inset image in the right showing the precipitates with higher magnification. The coating matrix comprises a hypoeutectic Al-Si chemical composition [30] and the precipitates were characterized as either Si or Al-Fe by means of an EDS mapping as shown in Fig. 2.

During hot-stamping processes, a chemical diffusion takes place and the coating becomes enriched in iron due to its diffusion from the steel substrate towards the coating layer [1,9,10,12,18]. Additionally, the precipitates at the top coating surface are no longer seen. However, cracks are observed at the PHS sample surface. These cracks, with preferential orientation at the surface, might be correlated to the plastic forming stage during the thermo-mechanical process, as seen in Fig. 1(b). The inset of Fig. 1(b) shows the cross-section of the PHS sample (further characterized in detail) with a crack present throughout the coating layer. As can be seen, the crack does not reach the steel substrate, but it is rather limited to the inter-diffusion layer. It is expected that the cracks will act as nucleation sites for localized corrosion which increases the susceptibility of damage and failure of the samples.

3.1.2. Cross section

The cross section of the as received Al-Si sample and the corresponding EDS mappings of qualitative chemical composition are shown in Fig. 2. The thickness of the coating layer is around 30 µm; and it is heterogeneous in terms of chemical composition. There are two sub layers from the steel substrate to the top layer and two different precipitates in the coating matrix. The first layer, also known as an inter-diffusion layer, is adjacent to the steel substrate and consists of an Al-Fe-Si ternary phase. The second layer, which is thicker than the first one, consists mainly of aluminium. This second layer is often named as a free coating layer or an outer layer [25]. Moreover, different

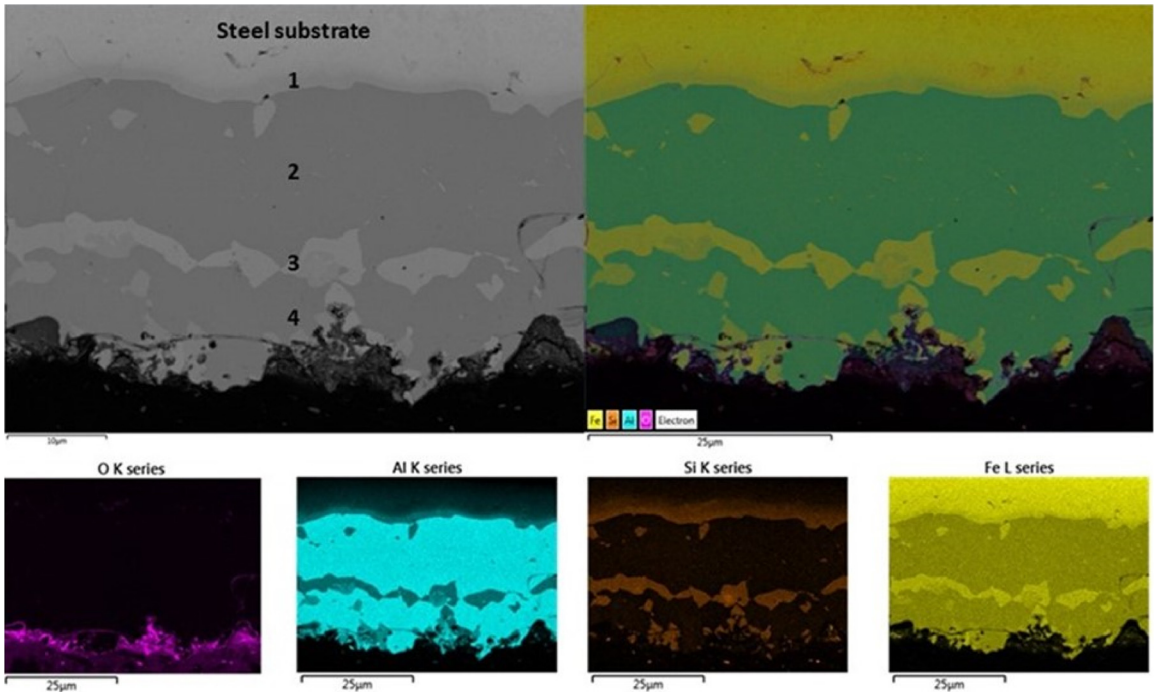

Fig. 3. Scanning backscattered images and EDS elemental mapping of the cross section of PHS sample condition for O, Al, Si and Fe.

precipitates are observed in the second layer some of which consist of pure silicon and others are composed of Al-Fe.

The hot-dip aluminized steels (HDA) have been extensively characterized [2,14,25,31–34]. However, there are many controversies regarding the characterization of the coating layer. The main reason is due to the different processing parameters used during the hot dip. The influence of the hot-stamping process on the coating morphology is shown in Fig. 3. It is seen that the coating microstructure consists of four sub layers with different chemical compositions. The layer, adjacent to steel substrate, as well as the third layer, consists of a Fe(rich)-Si-Al phase whereas the second and fourth layers are composed of an Al (rich)-Fe-Si phase.

The EDS mapping from Fig. 3 shows an oxygen-rich region at the sample's surface. There is a lack in literature about the nature of the oxide layer for PHS coated with Al-Si. Most of the studies have focused on the effect of the formation of Fe-based oxides at the surface of bare steel on the Al-Si coating adhesion, showing that it is detrimental [35]. Fan et al. [18] investigated the formation of thermal oxides on PHS coated with Al-Si. They pointed out that the oxidation is very limited due to the low diffusivity of oxygen throughout the coating layer. In addition, Fan et al. [12] highlighted the influence of the oxide layer of PHS on the resistance spot-welding (RSW) process, demonstrating that, due to its small thickness and good electrical conductivity of the Al-Fe phases, the PHS coated with Al-Si shows good welding properties. It is essential a careful investigation concerning the nature of the oxide layer formed after hot-stamping. Due to the iron enrichment during the thermo-mechanical process, it is expected a mixture of Al and Fe-based oxides. This oxide layer may play a role of protective barrier against corrosion.

As seen in Fig. 3, hot stamping of Al-Si coated 22MnB5 steel results in large changes in the coating layer. Its thickness increased about 10 µm and the morphology changed due to iron diffusion from the steel substrate towards the coating layer. It is important to point out that, before hot stamping, silicon was seen as pure precipitates in the coating matrix but, during the thermo-mechanical process, it was rearranged in different sub layers. The influence of silicon addition in HDA steels, used for hot-stamping applications, was intensively discussed by Windmann et al. [2,14]. Silicon plays an important role on the formation of Fe-Al intermetallic compounds. The transformation of these compounds has a direct relationship with the hot-dip parameters, such as soaking time and temperature during the austenitization step on hot stamping. The formation of $Al_{13}Fe_4$ (θ-phase) is attributed to the silicon amount [31,36]; the higher the addition of silicon, the more pronounced the formation of ternary Al-Fe-Si intermetallics and the more reduced the rate formation of $Al_{13}Fe_4$. In addition, as other authors pointed out, silicon suppresses the formation of Al_5Fe_2 (η-phase), occupying the vacancies in its lattice [31,36].

Despite the contradictions regarding the most accurate stoichiometry for those intermetallic compounds formed in press-hardened steel, there is an agreement that the number of sub layers formed is strongly dependent on the process parameters (soaking time and temperature). Moreover, it is known that the formed sub layers are either

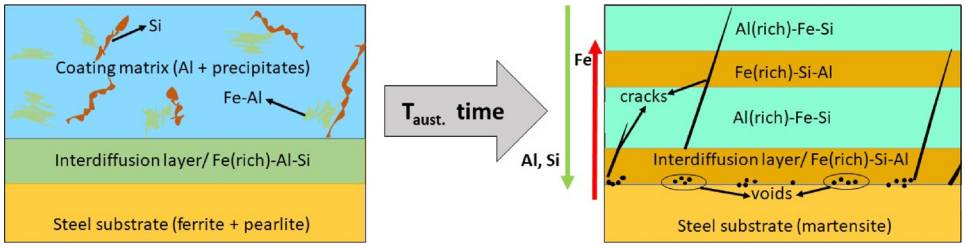

Fig. 4. Schematic of the changes on Al-Si coating morphology due to the chemical diffusion as a function of hot-stamping parameters illustrating the formation of intermetallic sub layers.

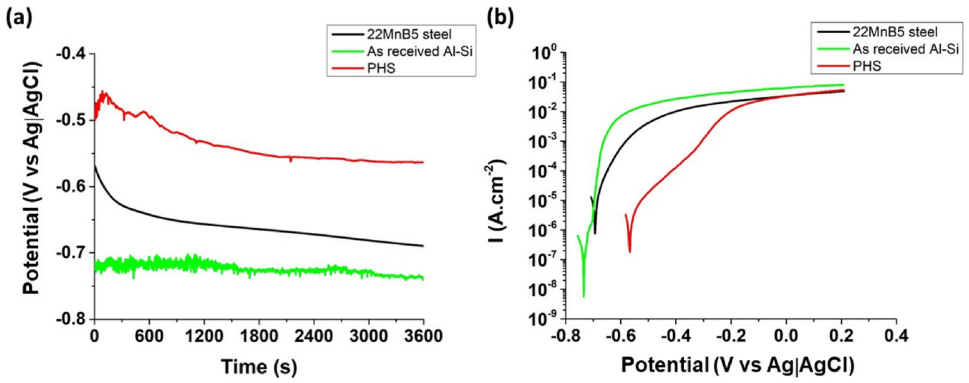

Fig. 5. Electrochemical tests in a 5 % NaCl solution (% in mass): (a) evolution of OCP for 1 h; (b) linear sweep voltammetry for the as received Al-Si, bare 22MnB5 steel and hot-stamped PHS samples.

enriched in iron or in aluminium [2,12,14], in accordance with the results showed in Fig. 3. Fig. 4 summarizes the changes on the coating morphology due to chemical diffusion which takes place during hot stamping.

Voids and micro cracks are also observed in the cross section of the PHS sample (Fig. 3), both related to the fast chemical diffusion during the hot-stamping process. The Kirkendall effect is very often pointed out in the literature as the reason for a void formation which is a consequence of the diffusivity difference of two atoms. The Kirkendall voids play a crucial role in crack initiation and it has been reported that the number of voids increases as the soaking time is prolonged. The cracks are also a consequence of the low fracture toughness of the sub layers which means that the sub layers formed after hot stamping are brittle, especially the ones enriched of aluminium [2,36–39].

3.2. Electrochemical measurements

Fig. 5 shows the evolution of OCP for 1 h of immersion in a 5.0 % NaCl solution (% in mass) and the anodic polarization curves obtained by linear sweep voltammetry (LSV) technique, after OCP measurements. According to Fig. 5(a), after 1 h of immersion, the OCP of all samples were stable. The OCP variation of the 22MnB5 steel sample, from the beginning to the end of measurements, was about 120 mV (versus Ag|AgCl 3 mol·L^{-1} KCl). Nevertheless, for the as received Al-Si and the PHS samples, these differences were around 10 mV and 60 mV, respectively. Considering the coated samples, as received Al-Si and PHS, the difference in OCP was initially about 220 mV, but after 1 h of test, the difference decreased to 170 mV. Despite the small variation in the OCP of the as received Al-Si sample, it shows the noisiest potential evolution among the tested conditions. This is a characteristic of metastable pits which consists of continuous localized breakdown and repassivation of the oxide layer. This behaviour is often observed in Al-Si systems in a chloride media [40]. The OCP of PHS sample is higher than that corresponding to the as received Al-Si one, suggesting that the driving force for cathodic protection might decrease after hot stamping. After 1 h of measurement, the OCP of the as received Al-Si sample had stabilized at around −730 mV, while that of the PHS sample stabilized at approximately -560 mV (both vs Ag|AgCl 3 mol·L^{-1} KCl). Nonetheless, the bare 22MnB5 steel sample presents OCP stable values between that of the PHS and of the as received Al-Si coated steel. This suggests that the Al-Si coating increases the susceptibility to corrosion of the steel exposed at the pores. The LSV results, Fig. 1(b), show that after hot stamping the corrosion potential (E^*) of Al-Si coated steel is shifted to nobler values. Concerning the corrosion potential, the galvanic series can be determined as follows: $E^*_{\text{as received}} < E^*_{\text{22MnB5 steel}} < E^*_{\text{PHS}}$.

The galvanic series suggests that, in terms of cathodic protection, only the Al-Si coating, before hot stamping, could behave as a sacrificial anode to the steel substrate. It is important to point out that these electrochemical measurements were performed at the surface of the samples. From the microscopic characterization, Figs. 1(a) and 2, it was shown that, before hot stamping, the coating matrix is mainly composed of aluminium which is less noble than iron, according to the galvanic series [20–24]. After the thermo-mechanical process, the top layer surface of the coating is enriched with iron due to the chemical diffusion during hot stamping. Thus, iron enrichment of the coating layer might be the reason for the nobler potential of the PHS sample when compared with the as received Al-Si. However, the iron enrichment does not justify the reason why the OCP of the PHS is higher than the bare steel. In this case, it could be attributed to the presence of an oxide layer formed during the hot stamping process as evidenced in Fig. 3. This oxide layer might play an extra role on the protection barrier mechanism, shifting the open circuit potential to nobler values.

Fig. 5(b) shows that all tested samples present an active behaviour. In terms of corrosion current, the as received Al-Si sample shows the lowest one. However, the current increases quickly in this sample condition in comparison with the others. According to Fig. 5(b), all the anodic curves stabilize in values very close to each other (0.06 A cm^{-2}), likely to the steel substrate exposure for those coated samples. Moreover, the anodic polarization curve for PHS sample condition increases slowly in comparison with the others. This could be due to the presence of Fe(rich)-Si-Al sub layers which might present a higher corrosion resistance than the other phases present. Another hypothesis is the presence of the oxide layer. After hot stamping, the corrosion potential is shifted to nobler value; however, the corrosion current is lower than the as received Al-Si sample. This is in agreement with the increase of OCP and, consequently, the decrease for cathodic protection.

The electrochemical results showed in Fig. 5 are slightly different from those presented by Allély et al. [3]. In their investigation, the PHS and 22MnB5 steel samples stabilized at similar OCP values (−770 mV vs SCE), after 1 h of measurement in a 5.0 % NaCl (% in mass) electrolyte. Hence, the OCP of as received Al-Si sample of the present work was about 100 mV lower. In terms of the corrosion potential, the galvanic series presented by them showed that the 22MnB5 bare steel presented the highest corrosion resistance, while the as received Al-Si sample condition showed the lowest. The controversies on the results can be probably explained by the process parameters used during hot stamping. As already mentioned, these parameters vary among manufacturers, influencing the diffusion of the chemical elements and, consequently, the coating morphology.

Several LSV measurements were carried out and Table 2 shows the average values of the corrosion potential as well as the standard deviation for the three conditions evaluated in two different solutions.

From the electrochemical results, it is seen that there is a negligible potential difference between the 22MnB5 uncoated and as received Al-Si coated. It means that there is no driving force for the Al-Si coating to

Table 2
Average corrosion potential obtained from DC anodic polarization curves of 22MnB5 steel, as received Al-Si and PHS samples condition in NaCl solution (5.0 % and 3.5 % in mass).

Samples condition	E^* (V vs Ag|AgCl 3 mol·L^{-1}) in 5 % NaCl (% in mass)		E^* (V vs Ag|AgCl 3 mol·L^{-1}) in 3.5 % NaCl (% in mass)	
	Mean value	Standard deviation	Mean value	Standard deviation
22MnB5 steel	−0.68	0.03	−0.67	0.03
as received Al-Si	−0.70	0.04	−0.68	0.01
PHS	−0.56	0.03	−0.54	0.05

provide cathodic protection to the steel substrate [3,6]. Allély et al. [3] pointed out that the minimum potential difference necessary to provide cathodic protection is 50 mV. Panossian et al. [41] found out that only in atmospheres with high chloride concentrations, Al and Al-Si coatings offer cathodic protection to steel substrates since the coatings passive properties are lost due to Cl^- ions. However, in chloride free atmospheres, or with very low ion concentrations, Al and Al-Si coatings preserve their passive properties due to the oxide layer on the metal surface.

It is important to highlight that in this case, the comparisons can be made only between the as received Al-Si condition and the 22MnB5 steel sample, because they have similar pearlite-ferrite steel microstructure, while the PHS condition has a fully martensitic microstructure. The difference of microstructure might also affect the electrochemical behaviour of the material. Kadowaki et al. [42] showed that martensite presents higher pitting corrosion resistance than ferrite and pearlite due to the presence of interstitial carbon. Interstitial carbon prevents both initiation and propagation of pitting. Moreover, they pointed out that iron carbides (Fe_3C - cementite) act as cathodic sites, increasing localized corrosion susceptibility.

3.2.1. Immersion test

In order to understand the influence of hot stamping on corrosion initiation, immersion tests were performed in a 3.5 % NaCl (% in mass) solution for 2 h. Fig. 6 shows the surface of the as received Al-Si coated and PHS samples before and after 2 h of immersion.

Fig. 6(a) shows the surface of the as received Al-Si coated sample and it is in agreement with the results previously presented in Fig. 1(a). The coating surface consists of an aluminium matrix with some Si and Al-Fe precipitates randomly distributed. After 2 h in chloride media, localized corrosion was observed at the sample surface, as shown in Fig. 6(b). The coating dissolution started around the precipitates which are either Si or Fe-Al precipitates and behave cathodically versus the matrix. These results are in agreement with those previously published [25]. However, for the PHS sample, Fig. 6(c) and (d) show no localized corrosion at the surface after hot stamping. However, red rust was seen at the surface of the sample using optical microscopy. As Dosdat et al. [6] pointed out the appearance of red rust is rather related to the high amount of iron at the top coating layer than to the coating damage. The suggested higher resistance to localized corrosion for the PHS sample might be attributed to the fact that the outer layer of the coating is composed of a homogeneous Fe-Al matrix without precipitates. It is important to notice that, even though cracks were seen in the PHS sample condition, they do not seem to play an active role in the corrosion process. Despite the presence of these cracks in the coating, the PHS presents the noblest potential and no localized corrosion.

3.3. Scanning Kelvin probe force microscopy

The scanning Kelvin probe force microscopy has been very often reported as a useful technique to evaluate the effect of alloy elements on the formation of intermetallic phase and its influence on corrosion mechanism [26,43–48]. As shown in Fig. 2 and in Fig. 3, both coated samples (as received Al-Si coated and PHS) consist of different intermetallic phases with different properties. This layered structure might play a crucial role on the corrosion mechanism.

The topographic map, the Volta potential map and a randomly chosen line profile across the coating for the as received Al-Si sample condition are shown in Fig. 7. From the topographic map, Fig. 7 (a), it is difficult to distinguish the two different layers present in the coating. However, these two layers and the precipitates can be easily distinguished in the Volta potential map (Fig. 7(b)). In addition, the Volta potential map shows the cathodic behaviour of the steel substrate versus the coating when exposed to air. The brighter contrast of the interdiffusion layer and the precipitates indicates that they are nobler than aluminium coating matrix which is in agreement with previously reported studies [25,26].

The Volta potential line profile, Fig. 7(c), shows that there is a high potential difference between the steel substrate and the coating layer; this difference is around 350 mV with the steel substrate being nobler than the coating layer which means that the coating could provide cathodic protection to the steel substrate. As already mentioned, the cathodic behaviour of Al-Si coatings depends on the concentration of chloride ions in the environment [41]. The Volta potential decreases across the coating layer which may be attributed to the decrease of iron content from the interdiffusion layer, grey highlight in Fig. 7 (c), towards the outer layer. Moreover, the potential varies in the coating layer due to the presence of different Fe-Al and Si precipitates characterized in Fig. 2. Both Volta potential map and line profile prove that the precipitates behave cathodically in comparison with the coating aluminium matrix. The precipitates act as cathodic sites where oxygen reduction reaction takes place. As already mentioned, the coating dissolution starts around these cathodic precipitates resulting in localized corrosion.

The histogram plot of the Volta potential map, from the cross section of the as received Al-Si sample, Fig. 7(b), is seen in Fig. 8. The histograms represent a multimodal Gaussian distribution. The peaks in the histograms might be correlated to different constituents at the area measured by means of SKPFM. Moreover, it is possible to evaluate the contribution of every different constituent on the Volta potential [46,49,50].

Fig. 8 shows that three different constituents contribute to the Volta potential distribution. The sharpest peak seen at the highest potential region, with an average value around −138 mV vs HOPG, is related to the steel substrate. The corresponding shape of the peak might be related to the major presence of iron in the steel substrate. If different constituents with different electrochemical activity are present around the same potential region, the peaks tend to be broader. The interdiffusion layer, which is composed of Fe-Al, presents a quite symmetric peak due to its composition homogeneity. The intensity is lower because it is a thinner layer in comparison with the steel substrate and the coating matrix, as clearly seen in Figs. 2 and 7(b). The potential of this interdiffusion layer has an average value around −263 mV vs HOPG. The peak corresponding to the Al-Si coating matrix is broader than the others, showing clear variations in Volta potential. The average potential value of the coating matrix was around −488 mV vs HOPG. Moreover, a tail-like shape, in the left side of this broader area, was observed. The findings from the histogram in Fig. 8 are in accordance with those previously reported by Sarvghad-Moghaddam et al. [49]. They have attributed the presence of precipitates in the Al matrix as the cause of the deviation in the Volta potential. In addition to this, the tail-like shape might be related to the aluminium signal, which is a less noble phase than the precipitates. As shown in the Volta potential line profile (Fig. 7(c)), the histogram (Fig. 8) confirms that the steel substrate has the noblest Volta potential, while the aluminium has the lowest one. The interdiffusion layer presents an intermediate potential, however, the Volta potential is shifted towards the Volta potential of the steel substrate due to the high amount of iron in this layer.

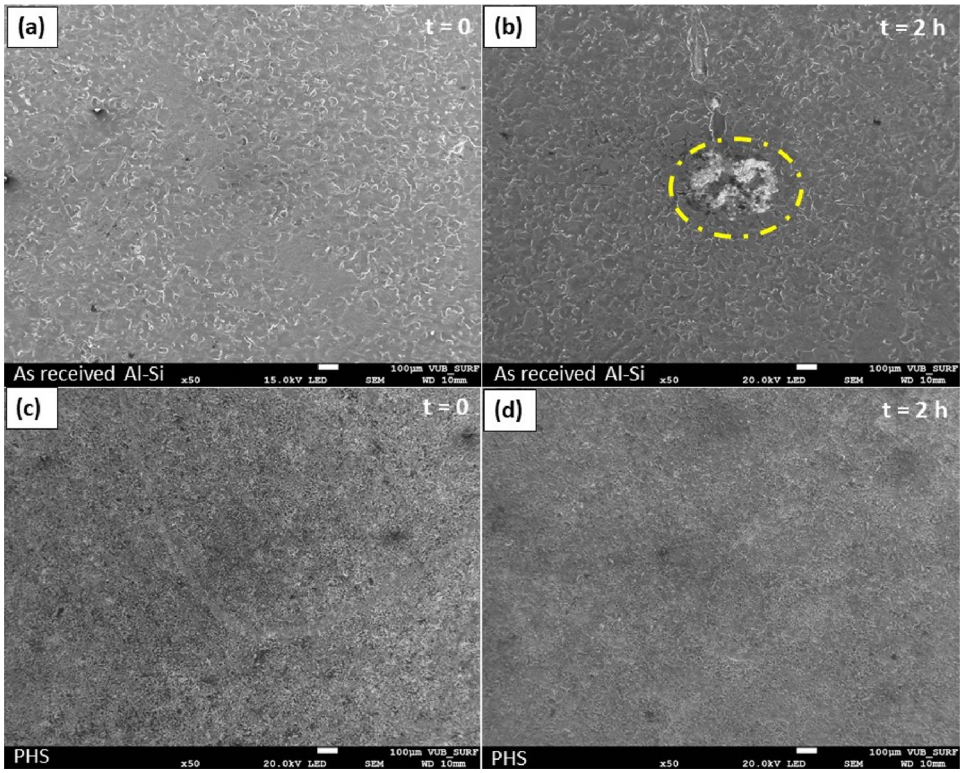

Fig. 6. Scanning secondary electron images of the surface before and after immersion in NaCl 3.5 % (a) as received Al-Si coated before immersion; (b) as received Al-Si coated after 2 h of immersion; (c) PHS before immersion; (d) PHS after 2 h of immersion.

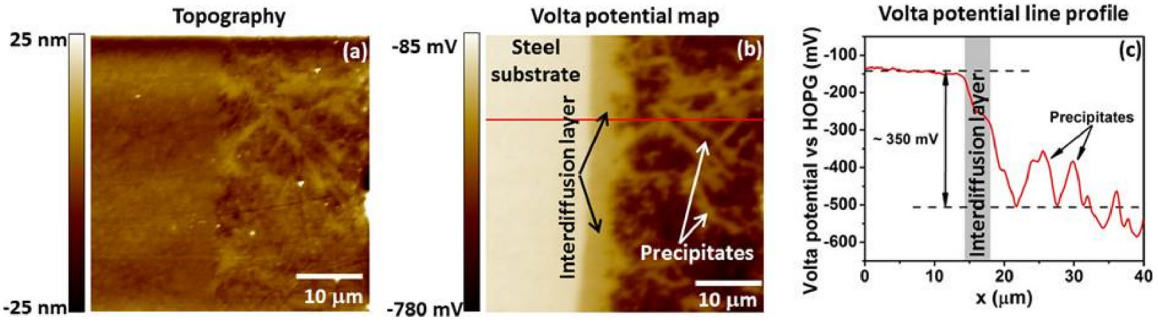

Fig. 7. Cross-section of 22MnB5 steel coated with hot-dip Al-Si prior hot-stamping process: (a) topographic map; (b) Volta potential map; (c) Volta potential line profile.

Fig. 9 shows the topographic map (a), the Volta potential map (b) and the Volta potential line profile (c) for a randomly chosen line from the Volta potential map. From the topographic map, Fig. 9(a), it is not clear the difference between the steel substrate and the coating layer. However, correlating the topographic map with the Volta potential map, Fig. 9(b), it is possible to distinguish a brighter contrast line which indicates the transition from the steel substrate to the coating layer. It is characterized as the interdiffusion layer, preferential site for Kirkendall voids formation [36]. From the Volta potential map, the cathodic behaviour of the steel substrate versus the coating layer is seen. Moreover, it is possible to differentiate the sub layers which comprise the coating. Correlating Figs. 3 and 9(b), it is seen that the brighter sub layers are corresponding to the Fe(rich)-Si-Al phases. Nevertheless, the contrast difference among the sub layers in the coating are not much pronounced. This indicates that there is no a high Volta potential difference among the sub layers, which is clear in Fig. 9(c), Volta potential line profile. In addition to this, according to Fig. 9(c) the Volta potential difference between the steel substrate and the coating greatly decreases after the hot-stamping process. This is associated with the iron diffusion during the hot-stamping process. After the thermo-mechanical process, the Volta potential difference between the steel substrate and the coating layer is approximately 66 mV. In addition, the potential difference among the sub layers in the coating is small, as already indicated by the contrast difference in Fig. 9(b).

The Volta potential decreases from the interface between the steel substrate and the coating layer (yellow highlight in Fig. 9(c)) due to the reduction in the amount of iron from the steel substrate towards the coating. The grey highlighted areas can be correlated to those Fe(rich)-Si-Al layers showed in Fig. 3 (sub layers 1 and 3). Due to the presence of iron and silicon, these layers show a slightly higher Volta potential in comparison with the other layer that is an Al(rich)-Fe-Si layer. As already mentioned, iron and silicon behave cathodically in comparison with aluminium which justifies the lower potential of the Al-rich sub layer. Due to the small differences of Volta potential among the sub layers, it is hard to establish an accurate potential difference. However, in order to evaluate the contribution of the sub layers, in terms of Volta potential, the histogram of the Volta potential map for the PHS sample is plotted in Fig. 10.

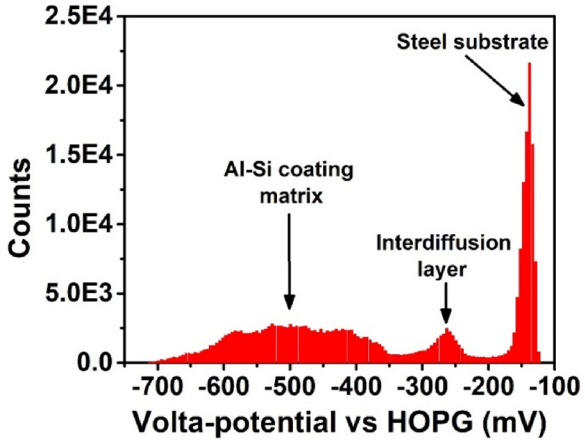

Fig. 8. Histogram of the distribution of Volta potential, based on the cross section Volta potential map of the as received Al-Si coated sample, showing the contribution of the three main areas: steel substrate, interdiffusion layer and Al-Si coating matrix.

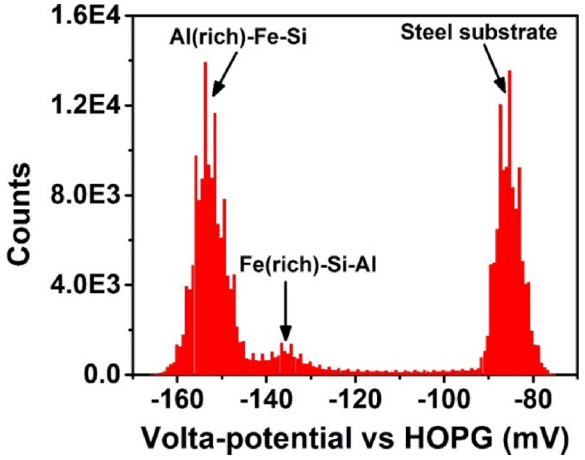

Fig. 10. Histogram of Volta potential distribution, based on the cross section Volta potential map, of the PHS sample, showing the contribution of the steel substrate and the two different sub layers: Fe(rich)-Si-Al and Al(rich)-Fe-Si.

Three different constituents are seen in the histogram (Fig. 10), which has a clear influence on the Volta potential distribution. The steel substrate and the Al(rich)-Fe-Si layer, which are the most abundant phases in the potential map shown in Fig. 9(c), can be identified as the two largest peaks in the histogram of Fig. 10. This is a consequence of the major influence of iron in the steel substrate and aluminium in the Al(rich)-Fe-Si layer. Additionally, they have the higher contribution on the Volta potential distribution due to their total area size in the sample cross section, as shown also in Fig. 3. The potential of the steel substrate is around −85 mV vs HOPG, while the average potential of the Al (rich)-Fe-Si layer (layer 2 in Fig. 3) is approximately −154 mV vs HOPG. However, the Fe(rich)-Si-Al sub layer is thinner and discontinuous, being probably the reason why the peak corresponding to Fe-rich phases is less sharp and much smaller than the others. Moreover, this phase has lower contribution on the Volta potential distribution than the others. The steel substrate shows a higher Volta potential than the two different sub layers in the coating. From the histogram, it is seen that the Volta potential of the two sub layers are close. The Volta potential difference between the Fe(rich)-Si-Al layer and the Al(rich)-Fe-Si layer is around 16 mV.

The hot-stamping process also changes the potential of the steel substrate and it might be correlated with the microstructure transformation during the thermo-mechanical process. Several SKPFM measurements were performed for both, as received Al-Si coated and PHS samples using HPOG as reference material. Fig. 11 shows the average Volta potential difference between the as received Al-Si coated and PHS steel substrates, with respect to HOPG. The difference is about 53 mV. Before hot stamping the steel substrate shows a ferrite-pearlite microstructure and its Volta potential is around -150 mV vs. HOPG. In the end

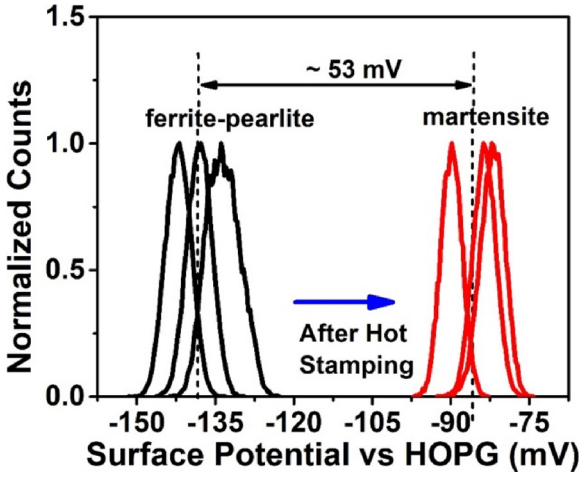

Fig. 11. Average Volta potential difference between as received Al-Si and PHS steel substrates measured versus the reference material.

of the thermo-mechanical process, a fully martensitic transformation takes place and the Volta potential of the martensite increases to approximately −90 mV vs. HOPG.

As the Volta potential is greatly influenced by any change in the sample surface and residual stress [28], it is possible to assume that the influence of different microstructures should be more noticeable in terms of Volta potential difference than corrosion potential difference, for instance. Moreover, related to the martensite transformation which results from the diffusionless transformation of austenite, implying,

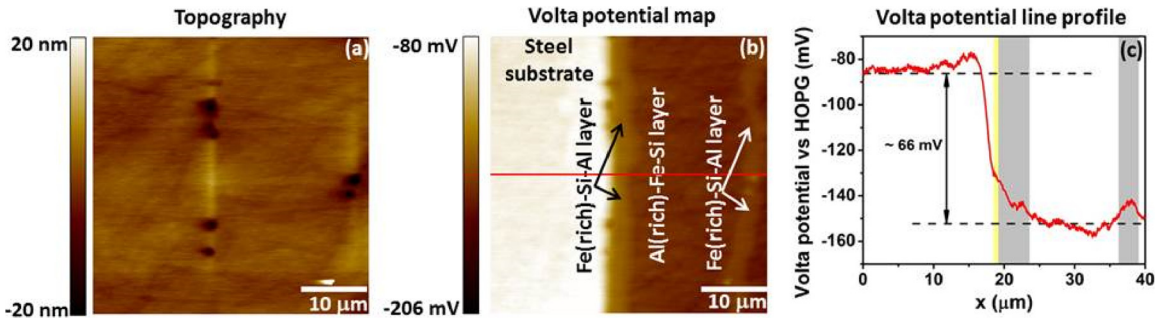

Fig. 9. Cross-section of hot-stamped 22MnB5 steel coated with hot-dip Al-Si (a) topographic map; (b) Volta potential map showing the different sub layers present in the coating; (c) Volta potential line profile.

very often, in residual stress on the material [51]. As already reported, the corrosion resistance of martensite is superior to the ferrite-pearlite structure due to the influence of interstitial carbon [42].

The Volta potential is often related to the corrosion potential. Many authors cite the study of Schmutz et al. [52] who found a linear relationship between the Volta potential and the corrosion potential for different metals. However, it is known that this behaviour has a strong dependence on the electrolyte [25]. In any case, the electrochemical measurements (Fig. 5) and the SKPFM results (Figs. 7 and 9) are in good agreement. The electrochemical results showed that the PHS presented nobler behaviour. In addition to this, from the SKPFM analysis, it is shown that the hot-stamping process enhances the Volta potential of the steel substrate and the coating layer. This might be attributed to a synergistic contribution, the microstructure transformation from ferrite-pearlite into martensite, and the iron diffusion from the steel substrate towards the coating layer.

Regarding cathodic protection, even though the coating layer of both samples, as received Al-Si coated and PHS, are less noble than their steel substrates, it has been shown that it depends on the environmental conditions and potential differences (either open circuit or corrosion potential) [3,41]. From the presented results, it is possible to assume that the hot-stamping process clearly decreased the driving force for cathodic protection of the substrate.

4. Conclusion

The hot-stamping process changes the coating morphology and, consequently, the electrochemical behaviour. The main findings can be summarized as follows:

1) After the thermo-mechanical process related to hot stamping, the coating layer became enriched in Fe and different sub layers were formed: Al(rich)-Fe-Si and Fe(rich)-Si-Al. Precipitates are no longer seen, decreasing the susceptibility for localized corrosion.
2) Electrochemical measurements showed that the PHS sample presented the noblest open circuit potential and corrosion potential and it presented the highest resistance to anodic polarization.
3) The local Volta potential showed that before hot stamping the pearlite-ferrite steel substrate is nobler than the coating layer. The coating consists of an interdiffusion layer enriched of iron and an aluminium matrix with Si and Al-Fe precipitates. The SKPFM results pointed out that the interdiffusion layer and the precipitates behave cathodically to the aluminium matrix.
4) After hot stamping, this Volta potential difference between the coating layer and steel substrate decreased from 350 mV to 66 mV. Besides the iron enrichment in the coating layer, the steel substrate was transformed into a fully martensite microstructure. The iron enrichment in the coating layer and the martensite are the reasons why the Volta potential difference decreased after hot stamping. SKPFM results showed a small difference in Volta potential among the sub layers in the PHS sample condition.
5) A concurrent mechanism was thoroughly established, i.e., while the press hardening enhances the corrosion properties of the steel system (steel and metallic coating) through diffusion, at the same time it diminishes the cathodic protection of the Al-Si layer.

CRediT authorship contribution statement

Camila Pucci Couto: Conceptualization, Writing - original draft, Investigation, Writing - review & editing. **Reynier I. Revilla:** Investigation, Formal analysis, Writing - review & editing. **Marco Antonio Colosio:** Funding acquisition, Resources. **Isolda Costa:** Conceptualization, Writing - review & editing. **Zehbour Panossian:** Writing - review & editing. **Iris De Graeve:** Conceptualization, Validation, Formal analysis, Writing - review & editing. **Herman Terryn:** Conceptualization, Methodology, Supervision, Writing - review & editing. **Jesualdo Luiz Rossi:** Conceptualization, Supervision, Writing - review & editing.

Declaration of Competing Interest

The authors declare that they have no known competing financial interests or personal relationships that could have appeared to influence the work reported in this paper.

Acknowledgments

The authors are grateful to the Coordination for Higher Education - Brazil (CAPES), process 88881.189691/2018-01, and National Council for Scientific and Technological Development (CNPq), process 205368/2018-2, for the scholarship granted to Camila Pucci Couto. In addition, the authors would like to thank Bart Lippens, for the samples cross-section preparation, Marc Raes and Priya Laha, for their assistance with FE-SEM-EDS. Finally, the authors thank the companies General Motors Mercosul and ArcelorMittal - Brazil, for materials' supply.

Appendix A. Supplementary data

Supplementary material related to this article can be found, in the online version, at doi:https://doi.org/10.1016/j.corsci.2020.108811.

References

[1] H. Karbasian, A.E. Tekkaya, A review on hot stamping, J. Mater. Process. Technol. 210 (2010) 2103–2118, https://doi.org/10.1016/j.jmatprotec.2010.07.019.
[2] M. Windmann, A. Röttger, W. Theisen, Phase formation at the interface between a boron alloyed steel substrate and an Al-rich coating, Surf. Coat. Technol. 226 (2013) 130–139, https://doi.org/10.1016/j.surfcoat.2013.03.045.
[3] C. Allély, L. Dosdat, O. Clauzeau, K. Ogle, P. Volovitch, Anticorrosion mechanisms of aluminized steel for hot stamping, Surf. Coat. Technol. 238 (2014) 188–196, https://doi.org/10.1016/j.surfcoat.2013.10.072.
[4] G. Venturato, M. Novella, S. Bruschi, A. Ghiotti, R. Shivpuri, Effects of phase transformation in hot stamping of 22MnB5 high strength steel, Proc. Eng. 183 (2017) 316–321, https://doi.org/10.1016/j.proeng.2017.04.045.
[5] M. Merklein, J. Lechler, Investigation of the thermo-mechanical properties of hot stamping steels, J. Mater. Process. Technol. 177 (2006) 452–455, https://doi.org/10.1016/j.jmatprotec.2006.03.233.
[6] L. Dosdat, J. Petitjean, T. Vietoris, O. Clauzeau, Corrosion resistance of different metallic coatings on press-hardened steels for automotive, Steel Res. Int. 82 (2011) 726–733, https://doi.org/10.1002/srin.201000291.
[7] J. Kondratiuk, P. Kuhn, E. Labrenz, C. Bischoff, Zinc coatings for hot sheet metal forming: comparison of phase evolution and microstructure during heat treatment, Surf. Coat. Technol. 205 (2011) 4141–4153, https://doi.org/10.1016/j.surfcoat.2011.03.002.
[8] R. Neugebauer, F. Schieck, S. Polster, A. Mosel, A. Rautenstrauch, J. Schönherr, N. Pierschel, Press hardening - an innovative and challenging technology, Arch. Civ. Mech. Eng. 12 (2012) 113–118, https://doi.org/10.1016/j.acme.2012.04.013.
[9] K. Mori, P.F.F. Bariani, B.-A.A. Behrens, A. Brosius, S. Bruschi, T. Maeno, M. Merklein, J. Yanagimoto, Hot stamping of ultra-high strength steel parts, CIRP Ann. Manuf. Technol. 66 (2017) 755–777, https://doi.org/10.1016/j.cirp.2017.05.007.
[10] D.W. Fan, H.S. Kim, S. Birosca, B.C. De Cooman, Critical review of hot stamping technology for automotive steels, Mater. Sci. Technol. Detroit (2007) 99–110.
[11] D.W. Fan, H.S. Kim, B.C. De Cooman, A review of the physical metallurgy related to the hot press forming of advanced high strength steel, Mater. Technol. 80 (2009) 218–222, https://doi.org/10.2374/SRI08SP131.
[12] D.W. Fan, B.C. De Cooman, State-of-the-knowledge on coating systems for hot stamped parts, Steel Res. Int. 83 (2012) 412–433, https://doi.org/10.1002/srin.201100292.
[13] A. Naganathan, L. Penter, Hot Stamping, ASM International, Chapter 7, Sheet Metal Forming - Processes and Applications, (2012), pp. 133–156 www.asminternational.org.
[14] M. Windmann, A. Röttger, W. Theisen, Formation of intermetallic phases in Al-coated hot-stamped 22MnB5 sheets in terms of coating thickness and Si content, Surf. Coat. Technol. 246 (2014) 17–25, https://doi.org/10.1016/j.surfcoat.2014.02.056.
[15] H. Järvinen, M. Isakov, T. Nyyssönen, M. Järvenpää, P. Peura, The effect of initial microstructure on the final properties of press hardened 22MnB5 steels, Mater. Sci. Eng. A 676 (2016) 109–120, https://doi.org/10.1016/j.msea.2016.08.096.
[16] L. Cho, H. Kang, C. Lee, B.C. De Cooman, Microstructure of liquid metal embrittlement cracks on Zn-coated 22MnB5 press-hardened steel, Scr. Mater. 90 (2014) 25–28, https://doi.org/10.1016/j.scriptamat.2014.07.008.
[17] C. Palm, R. Vollmer, J. Aspacher, M. Gharbi, Increasing performance of hot

stamping systems, Proc. Eng. 207 (2017) 765–770, https://doi.org/10.1016/J.PROENG.2017.10.826.
[18] D.W. Fan, H.S. Kim, J.-K. Oh, K.-G. Chin, B.C. De Cooman, Coating degradation in hot press forming, ISIJ Int. 50 (2010) 561–568, https://doi.org/10.2355/isijinternational.50.561.
[19] K.R. Jo, L. Cho, D.H. Sulistiyo, E.J. Seo, S.W. Kim, B.C. De Cooman, Effects of Al-Si coating and Zn coating on the hydrogen uptake and embrittlement of ultra-high strength press-hardened steel, Surf. Coat. Technol. 374 (2019) 1108–1119, https://doi.org/10.1016/j.surfcoat.2019.06.047.
[20] V. Gentil, Corrosion (in Portuguese), 3rd ed., LTC, Rio de Janeiro, 1996.
[21] M.G. Fontana, Corrosion engineering, McGraw-Hill Series in Materials Science and Engineering, New York, 3rd ed., (2005) ISBN 10: 0070607443.
[22] S. Wolynec, Electrochemical Techniques for Corrosion (in Portuguese), 1st ed., EDUSP, São Paulo, 2003 ISBN: 8531407494.
[23] J. Stephen, D. Cramer, B.S. Covino, Corrosion: fundamentals, testing, and protection, ASM Handbook 13A, ASM International, 2003.
[24] L.L. Shreir, R.A. Jarman, G.T. Burstein, Corrosion, 3rd ed., Elsevier, 1994, https://doi.org/10.1016/C2009-0-24066-9.
[25] I. De Graeve, I. Schoukens, A. Lanzutti, F. Andreatta, A. Alvarez-Pampliega, J. De Strycker, L. Fedrizzi, H. Terryn, Mechanism of corrosion protection of hot-dip aluminium-silicon coatings on steel studied by electrochemical depth profiling, Corros. Sci. 76 (2013) 325–336, https://doi.org/10.1016/j.corsci.2013.07.005.
[26] L.E. Fratila-Apachitei, I. Apachitei, J. Duszczyk, Characterization of cast AlSi(Cu) alloys by scanning Kelvin probe force microscopy, Electrochim. Acta 51 (2006) 5892–5896, https://doi.org/10.1016/j.electacta.2006.03.027.
[27] R.I. Revilla, H. Terryn, I. De Graeve, On the use of SKPFM for in situ studies of the repassivation of the native oxide film on aluminium in air, Electrochem. Commun. 93 (2018) 162–165, https://doi.org/10.1016/j.elecom.2018.07.010.
[28] C. Örnek, D.L. Engelberg, SKPFM measured Volta potential correlated with strain localisation in microstructure to understand corrosion susceptibility of cold-rolled grade 2205 duplex stainless steel, Corros. Sci. 99 (2015) 164–171, https://doi.org/10.1016/j.corsci.2015.06.035.
[29] C. Örnek, C. Leygraf, J. Pan, On the Volta potential measured by SKPFM–fundamental and practical aspects with relevance to corrosion science, Corros. Eng. Sci. Technol. 54 (2019) 185–198, https://doi.org/10.1080/1478422X.2019.1583436.
[30] C.P. Couto, M.A. Colosio, I. Costa, L.P. Barbosa, Z. Panossian, J.L. Rossi, Characterization of 22MnB5 steel metallic coated with either hot-dip AlSi or electroplated ZnNi before and after hot stamping, SAE Tech. Pap. (2018), https://doi.org/10.4271/2018-36-0074.
[31] W.-J. Cheng, C.-J. Wang, Growth of intermetallic layer in the aluminide mild steel during hot-dipping, Surf. Coat. Technol. 204 (2009) 824–828, https://doi.org/10.1016/j.surfcoat.2009.09.061.
[32] W.-J. Cheng, C.-J. Wang, Microstructural evolution of intermetallic layer in hot-dipped aluminide mild steel with silicon addition, Surf. Coat. Technol. 205 (2011) 4726–4731, https://doi.org/10.1016/j.surfcoat.2011.04.061.
[33] B. Lemmens, Y. Gonzalez Garcia, B. Corlu, J. De Strycker, I. De Graeve, K. Verbeken, Study of the electrochemical behaviour of aluminized steel, Surf. Coat. Technol. 260 (2014) 34–38, https://doi.org/10.1016/j.surfcoat.2014.06.064.
[34] B. Lemmens, H. Springer, I. De Graeve, J. De Strycker, D. Raabe, K. Verbeken, Effect of silicon on the microstructure and growth kinetics of intermetallic phases formed during hot-dip aluminizing of ferritic steel, Surf. Coat. Technol. 319 (2017) 104–109, https://doi.org/10.1016/j.surfcoat.2017.03.040.
[35] Z.-x. Gui, W.-k. Liang, Y.-s. Zhang, Formability of aluminum-silicon coated boron steel in hot stamping process, Trans. Nonferrous Met. Soc. China (English Ed.) 24 (2014) 1750–1757, https://doi.org/10.1016/S1003-6326(14)63249-0.
[36] Z.-X. Gui, K. Wang, Y.-S. Zhang, B. Zhu, Cracking and interfacial debonding of the Al-Si coating in hot stamping of pre-coated boron steel, Appl. Surf. Sci. 316 (2014) 595–603, https://doi.org/10.1016/J.APSUSC.2014.08.043.
[37] T. Maitra, S.P. Gupta, Intermetallic compound formation in Fe-Al-Si ternary system: part II, Mater. Charact. 49 (2003) 293–311, https://doi.org/10.1016/S1044-5803(03)00005-6.
[38] H. Springer, A. Kostka, E.J.J. Payton, D. Raabe, A. Kaysser-Pyzalla, G. Eggeler, On the formation and growth of intermetallic phases during interdiffusion between low-carbon steel and aluminum alloys, Acta Mater. 59 (2011) 1586–1600, https://doi.org/10.1016/j.actamat.2010.11.023.
[39] I. Yakubtsov, R. Sohmshetty, Evolution of Al-Si Coating microstructure during heat-treatment of Usibor® 1500, IOP Conf. Ser. Mater. Sci. Eng. 418 (2018) 1–8, https://doi.org/10.1088/1757-899X/418/1/012015.
[40] R.I. Revilla, J. Liang, S. Godet, I. De Graeve, Local Corrosion behavior of additive manufactured AlSiMg alloy assessed by SEM and SKPFM, J. Electrochem. Soc. 164 (2016) C27–C35, https://doi.org/10.1149/2.0461702jes.
[41] Z. Panossian, L. Mariaca, M. Morcillo, S. Flores, J. Rocha, J.J. Peña, F. Herrera, F. Corvo, M. Sanchez, O.T. Rincon, G. Pridybailo, J. Simancas, Steel cathodic protection afforded by zinc, aluminium and zinc/aluminium alloy coatings in the atmosphere, Surf. Coat. Technol. 190 (2005) 244–248, https://doi.org/10.1016/j.surfcoat.2004.04.023.
[42] M. Kadowaki, I. Muto, Y. Sugawara, T. Doi, K. Kawano, N. Hara, Pitting corrosion resistance of martensite of AISI 1045 steel and the beneficial role of interstitial carbon, J. Electrochem. Soc. 164 (2017) 962–972, https://doi.org/10.1149/2.0541714jes.
[43] M. Rohwerder, F. Turcu, High-resolution Kelvin probe microscopy in corrosion science: scanning Kelvin probe force microscopy (SKPFM) versus classical scanning Kelvin probe (SKP), Electrochim. Acta 53 (2007) 290–299, https://doi.org/10.1016/j.electacta.2007.03.016.
[44] K.A. Yasakau, A.N. Salak, M.L. Zheludkevich, M.G.S.S. Ferreira, Volta potential of oxidized aluminum studied by scanning Kelvin probe force microscopy, J. Phys. Chem. C 114 (2010) 8474–8484, https://doi.org/10.1021/jp1011044.
[45] F. Andreatta, L. Fedrizzi, The use of the electrochemical micro-cell for the investigation of corrosion phenomena, Electrochim. Acta 203 (2016) 337–349, https://doi.org/10.1016/j.electacta.2016.01.099.
[46] Z. Esfahani, E. Rahimi, M. Sarvghad, A. Rafsanjani-Abbasi, A. Davoodi, Correlation between the histogram and power spectral density analysis of AFM and SKPFM images in an AA7023/AA5083 FSW joint, J. Alloys. Compd. 744 (2018) 174–181, https://doi.org/10.1016/j.jallcom.2018.02.106.
[47] F.N. Afshar, J.H.W. De Wit, H. Terryn, J.M.C. Mol, Kelvin probe force microscopy as a means of predicting the electrochemical characteristics of the surface of a modified AA4xxx/AA3xxx (Al alloys) brazing sheet, Electrochim. Acta 88 (2013) 330–339, https://doi.org/10.1016/j.electacta.2012.10.051.
[48] Y. Jin, M. Liu, C. Zhang, C. Leygraf, L. Wen, J. Pan, First-principle calculation of Volta potential of intermetallic particles in aluminum alloys and practical implications, J. Electrochem. Soc. 164 (2017) C465–C473, https://doi.org/10.1149/2.0191709jes.
[49] M. Sarvghad-Moghaddam, R. Parvizi, A. Davoodi, M. Haddad-Sabzevar, A. Imani, Establishing a correlation between interfacial microstructures and corrosion initiation sites in Al/Cu joints by SEM-EDS and AFM-SKPFM, Corros. Sci. 79 (2014) 148–158, https://doi.org/10.1016/j.corsci.2013.10.039.
[50] A. Davoodi, Z. Esfahani, M. Sarvghad, Microstructure and corrosion characterization of the interfacial region in dissimilar friction stir welded AA5083 to AA7023, Corros. Sci. 107 (2016) 133–144, https://doi.org/10.1016/j.corsci.2016.02.027.
[51] W.D. Callister, D.G. Rethwisch, Fundamentals of Materials Science and Engineering: an Integrated Approach, 3rd, ed., John Wiley & Sons, Hoboken, NJ, 2008 ISBN 10: 0470343664.
[52] P. Schmutz, G.S. Frankel, Characterization of AA2024-T3 by scanning Kelvin probe force microscopy, J. Electrochem. Soc. 145 (1998) 2285–2295, https://doi.org/10.1149/1.1838633.